Composite Structures 279 (2022) 114729

Contents lists available at ScienceDirect

Composite Structures

journal homepage: www.elsevier.com/locate/compstruct

4D printing of shape memory polybutylene succinate/polylactic acid (PBS/PLA) and its potential applications

Cheng Lin [a], Liwu Liu [a,*], Yanju Liu [a], Jinsong Leng [b,*]

[a] Department of Astronautical Science and Mechanics, Harbin Institute of Technology (HIT), P.O. Box 301, No. 92 West Dazhi Street, Harbin 150001, People's Republic of China

[b] Center for Composite Materials and Structures, Harbin Institute of Technology (HIT), No. 2 Yikuang Street, P.O. Box 3011, Harbin 150080, People's Republic of China

ARTICLE INFO

Keywords:
4D printing
Shape memory polymers
PBS/PLA composite filaments
Near-infrared (NIR) light-responsive

ABSTRACT

4D printing adds time as the fourth dimension to 3D printing, which has been actively explored in the biomedical field to develop patient-specific implants due to the ease of manufacturing complex architectures and the capability of dynamic transformations. However, the 4D printing filament used for fused deposition modeling (FDM) is quite limited. Here, 4D printing shape memory polybutylene succinate/polylactic acid (PBS/PLA) composite filament is prepared. The mechanical properties, surface morphology, and shape memory performances of the printed specimens are investigated. Besides, graphene oxide functionalized PBS/PLA shows attractive photothermal properties under near-infrared (NIR) irradiation, and a dynamic, remote, and accurate controlled 4D transformation of a porous scaffold is exhibited. As the first demonstration of 4D printing filament of PBS/PLA for FDM, this work shows its promising application prospects in tissue engineering, photothermal therapy, etc. Additionally, NIR-triggered 4D transformation solves the problem that the conventional thermal-trigger transformation process is difficult to control.

1. Introduction

4D printing is a next-generation rapid prototyping method that integrates 3D printing (also known as additive manufacturing) and active materials to enable printed architectures to transform over time [1–3]. Shape memory polymer (SMP) is a typical and commonly used 4D printing active material, which can be transformed into a temporary configuration and fixed, and then recovered to the original (permanent) configuration under external stimuli, such as magnetic field, solution, heat, and light [4–8]. Therefore, 4D printing not only provides the opportunity to manufacture architectures with complexity and fineness, but also allows architectures to be programmed to change configurations, features, and functions [9]. Due to these unique advantages, 4D printing has been actively explored in the fields of soft robotics, wearable electronics, biomedical devices, etc. [4,10,11]. For biomedical applications, this technology is more attractive because of the ability to manufacture patient-customized medical devices and the possibility of dynamic and controllable structural transformation to meet different needs [12–21]. Zarek et al. fabricated a personalized shape memory 4D airway stent using PCL-based resin, which was expected to reduce migration and ensure stable anchoring. In addition, the low profile of the compressed SMP structure allowed for less damaging deployment [22]. Besides, customized 4D printing occlusion devices were developed for congenital heart disease, whose temporary configuration was designed as a straight geometry to facilitate interventional therapy. After reaching the target location, the device automatically recovered to a double-disc configuration to seal the defect. The customized device allowed ideal matching with the defect, which was conducive to increasing the occlusion success rate [9].

Polylactic acid (PLA) is a hydrophobic aliphatic polyester derived from renewable resources, which can be obtained via direct condensation of lactic acid and ring-opening polymerization of lactide [23]. Because of its high strength, high modulus, biodegradability, and biocompatibility, it has aroused widespread research interests and is considered to be one of the most promising biomaterials. It has been widely used in drug delivery systems, implantable scaffolds, wound treatment, sutures, embolization devices, etc. [9,24–29]. However, the inherent brittleness of PLA has greatly hindered its wide application in many fields. Studies have shown that blending with tough polymers can enhance the elasticity of PLA [30]. Polybutylene succinate (PBS) is an aliphatic polyester with excellent ductility at room temperature, and the elongation at break may exceed 300% [31,32]. It is completely bio-

* Corresponding authors.
E-mail addresses: liuliwu_006@163.com (L. Liu), lengjs@hit.edu.cn (J. Leng).

https://doi.org/10.1016/j.compstruct.2021.114729
Received 19 July 2021; Received in revised form 17 September 2021; Accepted 23 September 2021
Available online 27 September 2021

based and bioabsorbable and can be synthesized by condensation polymerization of raw materials (1, 4-butanediol and succinic acid) from renewable resources. These characteristics enable PBS to be an appealing polymer for biomedical applications, and it has been used in tissue engineering and controlled drug release [33]. Therefore, the combination of PBS and PLA is a good choice for balancing strength and ductility. More importantly, due to thermoplasticity and processability, PBS/PLA blend may be a desirable candidate biomaterial for additive manufacturing with excellent biodegradability and biocompatibility.

Fused deposition modeling (FDM) is a filament-based 3D printing technology, the schematic of FDM is illustrated in Fig. 1a. The thermoplastic filament is melted by a heating head and extruded through a nozzle with a certain diameter, and then the material is deposited layer by layer on the platform according to the computer model to obtain various architectures. FDM is considered to be the most widely used 3D printing technology, with advantages of low cost, space saving, and ease of operation [34]. The commercialized 3D printing filaments for FDM include polylactic acid (PLA), polyamide (PA, nylon), acrylonitrile butadiene styrene (ABS), polyvinyl alcohol (PVA), polyethylene terephthalate (PET), polycaprolactone (PCL), etc. In addition, there are some works on the fabrication of FDM 3D printing composite filaments, such as PCL/PLA [35], MWCNTs (multiwall carbon nanotubes)/ABS [36], short glass fiber/PP [37]. Although the FDM 3D printing filaments are diverse, 4D printing filaments are quite limited and their functions are less involved. The lack of advanced printable and functional intelligent filament materials has significantly limited the development of FDM-based 4D printing technology.

The aim here was to develop a 4D printing composite filament for FDM to enrich the diversity of materials, to dynamically, remotely, and accurately control the 4D transformation process, and to demonstrate its

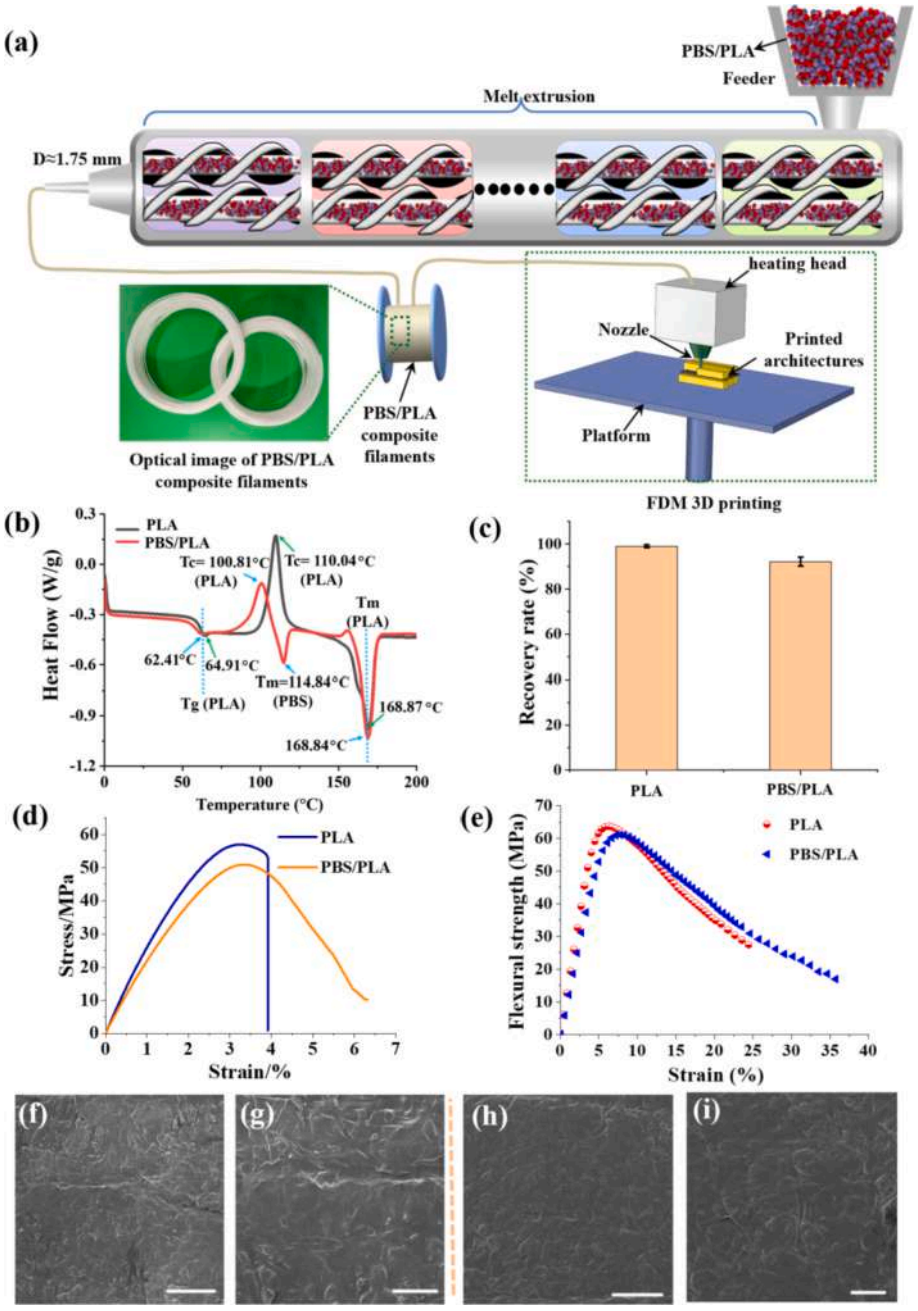

Fig. 1. (a) Preparation of PBS/PLA composite filaments and the schematic of FDM 3D printing. (b) DSC patterns. (c) Shape memory performances. (d) Uniaxial tensile tests. (e) Three-point bending tests. Surface morphology of printed (f, g) PLA and (h, i) PBS/PLA specimens. Scale bars: 500 μm (f, h); 200 μm (g, i).

potential in biomedical applications. First, PLA and PBS/PLA 4D printing filaments were prepared by melt extrusion. Then the tensile/flexural properties, surface morphology, thermal behaviors, and shape memory performances were systematically examined. Various complex 3D architectures were constructed and printed with high quality using the PBS/PLA filaments through a commercial FDM 3D printer, showing good printability of PBS/PLA filaments. In addition, a coil used for embolization was designed and its 4D transformation process was investigated in a printed aneurysm model. Finally, graphene oxide (GO) was employed to functionalize PBS/PLA to achieve near-infrared (NIR) light-responsive 4D transformation. GO is a 2D carbon atom sheet with a honeycomb structure, which has excellent photothermal performance, high thermal conductivity, and favorable biocompatibility. GO has shown tremendous potential applications in biotechnology, such as photothermal anticancer therapy [38], drug delivery [39], bioassay, etc. [40–42]. Under the irradiation of NIR laser, GO can absorb photons and convert them into heat. The photothermal effects of GO functionalized PBS/PLA specimens irradiated by NIR laser with different power densities were studied. Besides, a GO functionalized PBS/PLA porous scaffold was prepared and its NIR-triggered 4D transformation was examined.

2. Experimental section

2.1. Preparation of PLA and PBS/PLA filaments

PLA pellets [9] and PBS powder (Xinjiang Blue Ridge Tunhe Chemical Industry Joint Stock Co., Ltd) were dried at 45 °C for 24 h and then physically mixed at a mass fraction ratio of 9:1. The mixture was melt-blended and extruded by an extruder and PBS/PLA composite filaments with a diameter of 1.75 ± 0.05 mm were obtained. Fig. 1a shows the melt extrusion process and the optical image of the PBS/PLA composite filaments. The PLA filaments were prepared by a similar method.

2.2. 4D printing of architectures

Various architectures were built via Siemens PLM software UG NX 10.0 and then exported as. STL files. Next, slicing software was employed to get the final. Gcode files. All architectures were printed using a commercial dual head 3D printer (Allcct, Wuhan, China). The printing temperature of PLA was set to 190 °C, and that of PBS/PLA was set to 210 °C. The filling density of tensile/flexural test specimens was 100% and that of other specimens was 20%. The nozzle diameter, printing speed, shell thickness, and layer height were 0.4 mm, 10 mm/s, 0.8 mm, and 0.1 mm, respectively.

2.3. Tensile/flexural properties

Tensile and flexural properties of specimens at room temperature (25 °C) were examined using Zwick-010 (Zwick Roell Group, Germany) according to ASTM D638 and ASTM D790. Three specimens of each type were tested at an operating speed of 2 mm/min until failure.

2.4. Morphology

The (fracture) surface morphology of the mechanical test specimens was investigated through scanning electron microscopy (SEM, VEGA3 TESCAN). Before the examination, the specimens were sputter-coated with a thin layer of gold and then observed at a voltage of 10 kV.

2.5. Differential scanning calorimeter (DSC)

A METTLER TOLEDO DSC was applied to examine the thermal properties of PLA and PBS/PLA. Specimens of approximately 7.0 mg were cut from the filaments, sealed in an Al pan, and then loaded into the chamber. Two rounds of tests were conducted at temperatures ranging from 0 °C to 200 °C under nitrogen, with heating and cooling rates of 10 °C/min. The second heating data was exported to draw the curves in Fig. 1b.

2.6. Examination of shape memory performances

The architecture (e.g., starfish, endoluminal stent, embolization coil, porous scaffold) was first placed in a hot water bath (glass transition temperature (T_g) + 20 °C) for 5 min, then programmed into a temporary configuration, and kept at room temperature (25 °C) for another 5 min. After the above process, the temporary configuration was fixed. Finally, the architecture in the temporary configuration was reheated and recovered to its original configuration automatically.

2.7. Preparation of GO-functionalized PBS/PLA specimens

GO (Shanghai SIMbatt Energy Technology Co., Ltd. GO) was mixed with distilled water and placed in an ultrasonic water bath for 200 min to obtain a uniform GO suspension (1 mg/ml). The printed PBS/PLA specimens were immersed in the prepared GO suspension for 15 min and then dried at 45 °C for 20 min. The process was repeated three times and the GO functionalized PBS/PLA specimens were obtained.

2.8. Photothermal effects of GO-functionalized PBS/PLA

GO functionalized PBS/PLA rectangular specimens were prepared to test photothermal effects (Fig. 6a) and irradiated with 808 nm NIR laser at different laser power densities (1, 2, 3, 5 W/cm^2) for 5 min. In addition, the compressed GO functionalized PBS/PLA porous scaffold was irradiated with the 808 nm NIR laser at a power density of 5 W/cm^2, and the NIR-triggered 4D transformation process was recorded. The temperature of the specimen was monitored in real time by the infrared thermal imaging system.

3. Results and discussion

3.1. Characterizations of PLA and PBS/PLA

The thermal behaviors of PLA and PBS/PLA were characterized by DSC (Fig. 1b). The T_g of PLA in the PBS/PLA blend was lower than that of PLA, which might be attributed to the good dispersion of PBS in the PLA matrix and the plasticizing effect of PBS on the PLA matrix. The cold crystallization peak (crystallization temperature, T_c) of PLA in the blend exhibited a significant shift to lower temperature because PBS acted as the nucleation site of PLA and contributed to the crystallization of PLA [43]. The melting point of PLA had no significant difference between PLA and PBS/PLA blend.

In addition, the shape memory performances of PLA and PBS/PLA were studied (Fig. 1c). A typical shape memory mechanism is as follows. The shape memory effect of SMP is attributed to the coexistence of hard segments (fixed phases) and soft segments (reversible phases). The movable and reversible soft segments determine the shape fixation performance of SMP, while the hard segments are responsible for the shape recovery performance of SMP due to their physical or chemical crosslinks. At room temperature, SMP is usually in a glassy state. When heated above the shape memory transition temperature (T_{trans}), the soft segments of SMP will enter a rubbery state and the mobility of the molecular chain will increase. In the rubbery state, SMP can easily be programmed into any desired temporary configuration. T_{trans} can be T_g or melting temperature (T_m), and for PLA, T_g acts as T_{trans}. When the applied load is maintained and the temperature of SMP is cooled below T_{trans}, the molecular chains of the soft segments will be frozen, the conformations of deformed chains will be fixed, and the entropy will be stored in the temporary configuration. When SMP is reheated, the entropy will be released and returned to the initial maximum entropy state. The fixed phases rely on physical or chemical cross-linking to enable

SMP to recover to its original configuration. The shape recovery rates of PLA and PBS/PLA were 99.04% and 92.19% (Fig. 1c), demonstrating their excellent shape memory performance, which was of great significance for SMP-based implantable scaffolds. Compared with PLA, the shape recovery rate of PBS/PLA decreased slightly, which might be attributed to the fact that the introduction of PBS hindered the formation of the physical crosslinking network formed by PLA chains entanglement, thus affecting the shape recovery performance.

Fig. 1d shows the stress–strain curves of PLA and PBS/PLA specimens under uniaxial tensile loading. Compared with PLA, the tensile strength of PBS/PLA decreased slightly, while the fracture strain increased visibly. The tensile strength and fracture strain of PLA and PBS/PLA were 56.963 MPa/50.934 MPa and 3.925%/6.316%. In addition, three-point bending tests were conducted to evaluate the flexural performance of the 4D printed PBS/PLA blend, as shown in Fig. 1e. Similar to the tensile tests, the flexural strength was slightly reduced, while the toughening effect of PBS/PLA specimens was significantly improved due to the presence of PBS. The surface morphology of the printed PBS/PLA and PLA specimens was examined (Fig. 1f-i) and the slight surface structure was partly due to the deposition of layers during FDM printing.

In addition, the fracture surface morphology of the tensile specimens and the three-point bending test specimens at different magnifications were studied, as displayed in Fig. 2. The PBS/PLA material can be stretched for a long distance along the loading direction (indicated by the yellow arrow in Fig. 2a-c), resulting in fibrous protrusions and large fracture strain. The fibrous protrusions connected two fracture surfaces that were not completely separated (Fig. 2a, c), that was, PBS/PLA was still partially continuous. The plastic fracture mode of PBS/PLA was attributed to the fact that partially continuous PBS/PLA can absorb more energy. In contrast, the fracture surface of PLA (Fig. 2d-f) was smoother with fewer features, corresponding to the brittle fracture mode and smaller fracture strain. The results of the fracture surface morphology were consistent with the mechanical test results in Fig. 1d, e.

3.2. 4D printed PBS/PLA architectures and potential applications

To verify the printability of the prepared PBS/PLA filaments, the starfish and endoluminal stent were developed (Fig. 3a1, b1). The structure of the endoluminal stent can be used for a vascular stent, tracheal stent, or intestinal stent, as long as it is printed according to the

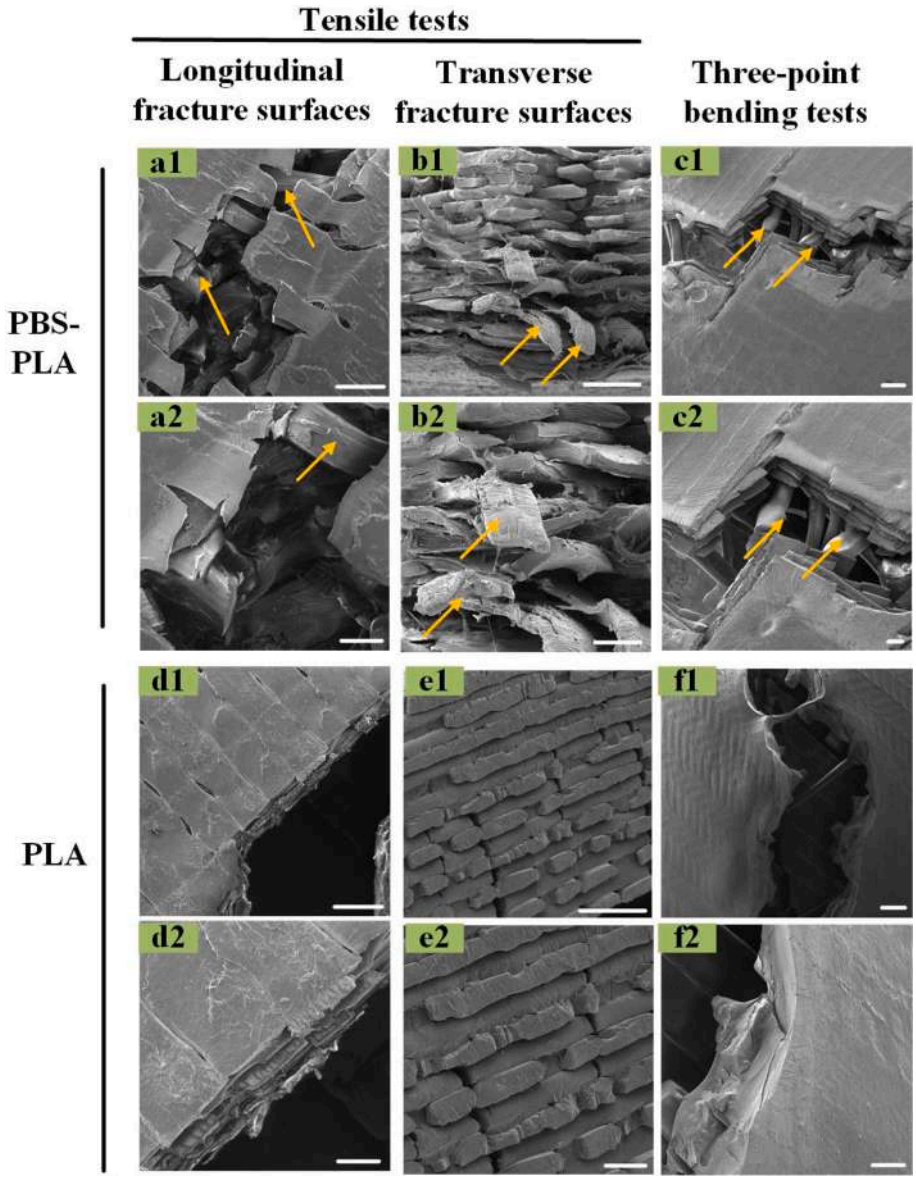

Fig. 2. SEM micrographs of 4D printed PBS/PLA and PLA specimens. (a, d) Longitudinal fracture surfaces of tensile specimens. (b, e) Transverse fracture surfaces of tensile specimens. (c, f) Fracture surfaces of three-point bending specimens. Scale bars: 500 μm (a1, b1, c1, d1, e1, f1); 200 μm (a2, b2, c2, d2, e2, f2).

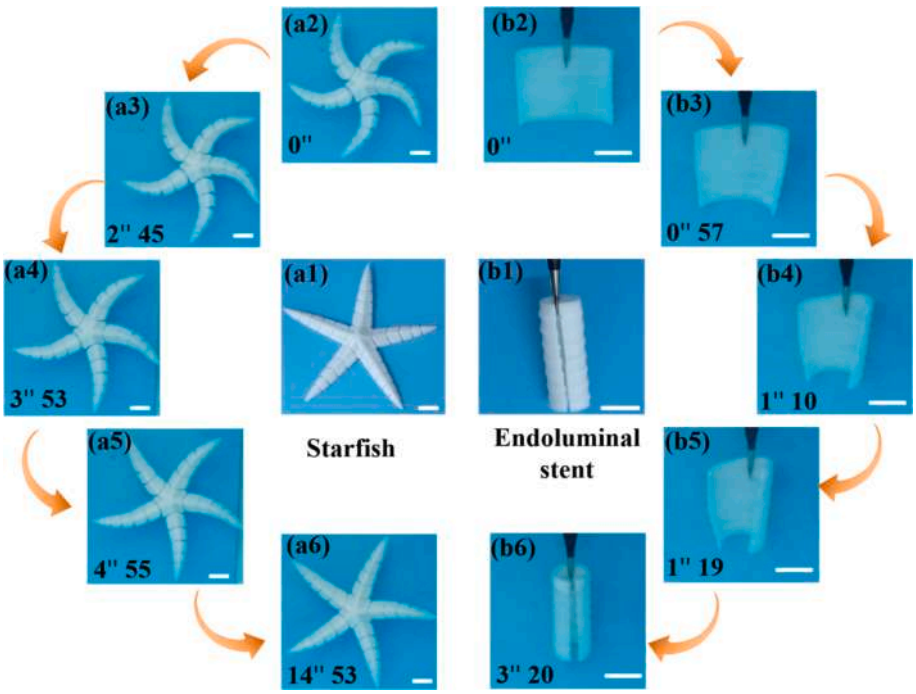

Fig. 3. Shape memory behaviors of 4D printed PBS/PLA architectures. (a) Starfish. (b) Endoluminal stent. (a1, b1) Permanent configurations. (a2, b2) Temporary configurations. (a2-a6, b2-b6) Shape recovery processes. Scale bars: 10 mm.

corresponding size. Fig. 3a1 and b1 show the permanent configurations of the starfish and endoluminal stent, and Fig. 3a2 and b2 are the temporary configurations after programming. The shape memory behaviors were investigated by placing temporarily shaped configurations in a hot water bath, and smooth and complete shape recovery processes can be observed (Fig. 3a2-a6, Fig. 3b2-b6). The difference in recovery time between the starfish and the endoluminal stent was attributed to their different configurations. The wall thickness of the starfish was much thicker than that of the endoluminal stent, thus it took more time for heat conduction and shape recovery.

In addition, the process of aneurysm embolization was demonstrated to further illustrate the potential application of PBS/PLA. An aneurysm is a localized dilation of the artery caused by a weakened or damaged blood vessel wall. Once rupture occurs, it will lead to catastrophic and fatal bleeding. Because of the high risk of open surgery such as craniotomy, endovascular interventional embolization has become the preferred treatment for aneurysms due to its safety and less trauma. The goal of embolization is to isolate the aneurysm sac from the blood circulation by delivering the embolic agent to the target sac, thus reducing the risk of rupture [44–46]. As shown in Fig. 4a, a coil was designed to be used as an embolic agent and printed using the prepared PBS/PLA filaments. The coil can be programmed to achieve a pronounced contraction into a straight strip, which was a temporary shape that facilitated interventional delivery (Fig. 4b). To evaluate the feasibility of coil deployment in the aneurysm, an aneurysm model was established and manufactured with PBS/PLA filaments. It can be observed that the aneurysm model was printed with high quality (Fig. 4c), further verifying the good printability of PBS/PLA filaments and the ability to manufacture complex configurations. To demonstrate the embolization process more clearly, the printed aneurysm model was colored to distinguish it from the coil (Fig. 4d).

Fig. 5 shows the embolization process of the PBS/PLA coil in the aneurysm model, and a hot water bath was used as the external stimulus. A 13Fr. interventional catheter was employed to deliver the stretched coil (temporary shape, strip). After positioning, the strip was gradually pushed out from the catheter through the guidewire, and the gradual shape recovery process can be observed. As shown in Fig. 5h, the coil

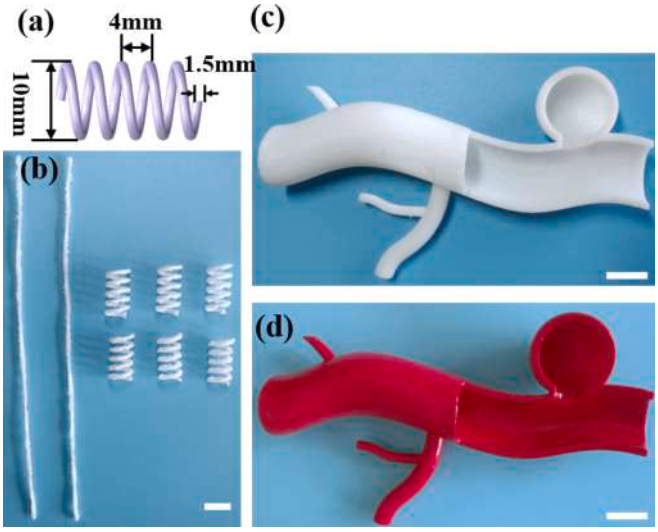

Fig. 4. (a) 3D model of the embolization coil. (b) Printed coils (right) and their temporary shapes (strips on the left). (c) Aneurysm model printed with PBS/PLA filaments. (d) Colored aneurysm model. Scale bar: 10 mm.

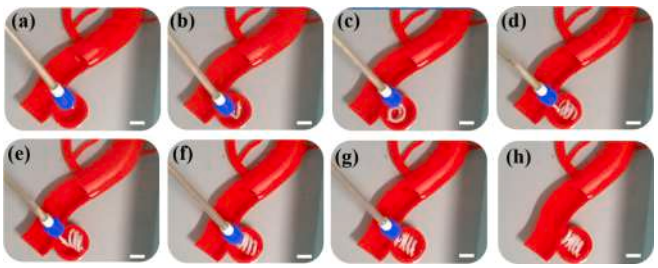

Fig. 5. Embolization process of the PBS/PLA coil in aneurysm model. Scale bar: 10 mm.

was completely filled into the sac and the embolization was accomplished. This process showed that the excellent shape memory effect of the coil ensured accurate deployment, which can solve the problem of poorly controlled embolization of gelatin sponge, the most common embolic agent.

3.3. GO-functionalized PBS/PLA and its photothermal effects

The photothermal effects of GO functionalized PBS/PLA specimens were investigated, and the NIR laser with a wavelength of 808 nm was employed as the light source, which can effectively penetrate the tissue without causing harm. Fig. 6a displays the printed PBS/PLA specimens before and after GO functionalization. The GO functionalized PBS/PLA specimens showed excellent photothermal performance under the irradiation of the NIR laser (Fig. 6b). The temperature of the GO functionalized PBS/PLA specimens increased with the increase of NIR laser power density. When the NIR laser power density was 1 W/cm^2, the maximum temperature of the GO functionalized PBS/PLA specimen after 300 s irradiation was approximately 39 °C. When the power density increased to 2 W/cm^2 and 3 W/cm^2, the maximum temperature rose to approximately 52 °C and 69 °C, respectively. Under the irradiation of NIR with a power density of 5 W/cm^2, the GO functionalized PBS/PLA specimen rapidly rose to about 60 °C within 60 s and reached 76 °C after 300 s. However, the PBS/PLA specimens without GO functionalization did not exhibit photothermal effects (Fig. 6c). The temperature increased slightly with power density, but the maximum temperature was only 38.5 °C (5 W/cm^2, 300 s). To display the temperature evolution of the specimens more intuitively, the corresponding infrared radiation thermal images are shown in Fig. 7. The central temperature of each thermal image in Fig. 7 is the temperature of the points with corresponding labels on the curves in Fig. 6b, c. For example, the central temperature of Fig. 7g4 corresponds to the temperature of point g4 on the curve (5 W/cm^2, GO-PBS/PLA) in Fig. 6b.

3.4. NIR-triggered 4D transformation of GO-functionalized PBS/PLA porous scaffold

To explore the feasibility of NIR triggering GO-functionalized PBS/PLA for 4D transformation, a porous scaffold with dimensions of 9 mm × 9 mm × 13 mm was designed and developed to facilitate bone regeneration. The porous scaffold was compressed, and its NIR-triggered 4D transformation behavior was evaluated by multiple position illumination (Fig. 8a, Movie S1). The results showed that the transformation of the porous scaffold can be controlled dynamically, remotely, and accurately by NIR laser irradiation. The temperature of the porous scaffold during the 4D transformation process was monitored by the infrared thermal imaging system (Fig. 8b). In the initial stage of irradiation, the temperature of the porous scaffold increased rapidly, then gradually balanced and fluctuated in the temperature range of approximately 50°C to 56°C. Compared with the GO functionalized PBS/PLA rectangular specimens (Fig. 6b), the porous scaffold exhibited a much lower temperature under the same power density of NIR laser irradiation. This phenomenon might be due to the fact that the temperature of the outer surface was monitored by the infrared thermal imaging system, while the internal temperature of the porous scaffold was higher than that of the outer surface due to the slower temperature dissipation rate.

Therefore, the advantages of the NIR-triggered 4D printed GO functionalized PBS/PLA can be summarized as follows. First, the compressed temporary configuration of the porous scaffold can reduce the scar area. Secondly, the self-adaptive ability can match the defects during the shape recovery process. Thirdly, a dynamic, accurate, and remotely controllable transformation process is accessible.

4. Conclusion

In summary, the 4D printing PBS/PLA filament was developed for the first time, and its outstanding printability was demonstrated by printing various configurations (e.g., starfish, endoluminal stent, aneurysm model) through a commercial 3D printer. The introduction of PBS improved the toughness of PBS/PLA compared to PLA without significant loss of modulus and strength. In addition, the embolization coil was printed and delivered by an interventional catheter. Its 4D transformation was performed in the printed aneurysm model, which indicated that the 4D printing PBS/PLA filament with excellent shape memory performance had a promising prospect in the biological field, especially in interventional surgery. GO functionalized PBS/PLA porous scaffold can be triggered by NIR laser, which enabled a dynamic, accurate, and remotely controllable 4D transformation in time and space. Besides, GO functionalized PBS/PLA showed excellent photothermal effects, indicating its potential for application in photodynamic therapy.

CRediT authorship contribution statement

Cheng Lin: Conceptualization, Methodology, Investigation, Writing – original draft, Visualization. **Liwu Liu:** Investigation, Validation, Supervision, Writing - review & editing. **Yanju Liu:** Supervision, Writing - review & editing, Resources, Project administration. **Jinsong Leng:** Supervision, Writing - review & editing, Resources, Funding acquisition.

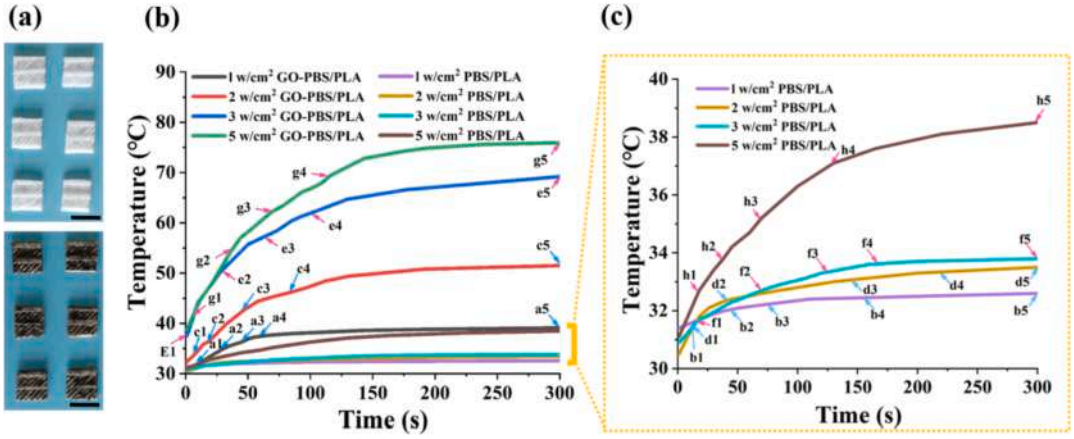

Fig. 6. (a) Printed PBS/PLA specimens before (white ones) and after (black ones) GO functionalization. Scale bar: 5 mm. (b) Temperature evolution of PBS/PLA and GO functionalized PBS/PLA specimens under NIR irradiation with different laser power densities. (c) Enlarged view of the temperature evolution of PBS/PLA specimens in (b).

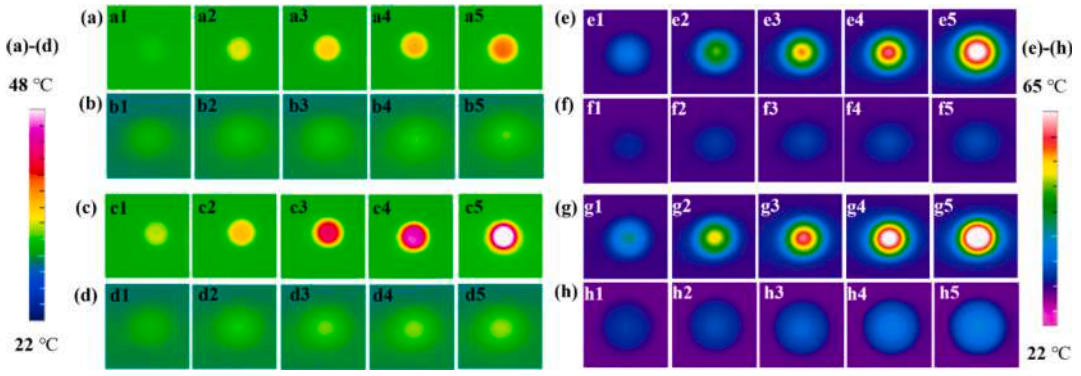

Fig. 7. Infrared radiation thermal images of GO functionalized PBS/PLA specimens irradiated by NIR laser at power densities of (a) 1 W/cm^2; (c) 2 W/cm^2; (e) 3 W/cm^2; (g) 5 W/cm^2. Infrared radiation thermal images of PBS/PLA specimens irradiated by NIR laser at power densities of (b) 1 W/cm^2; (d) 2 W/cm^2; (f) 3 W/cm^2; (h) 5 W/cm^2.

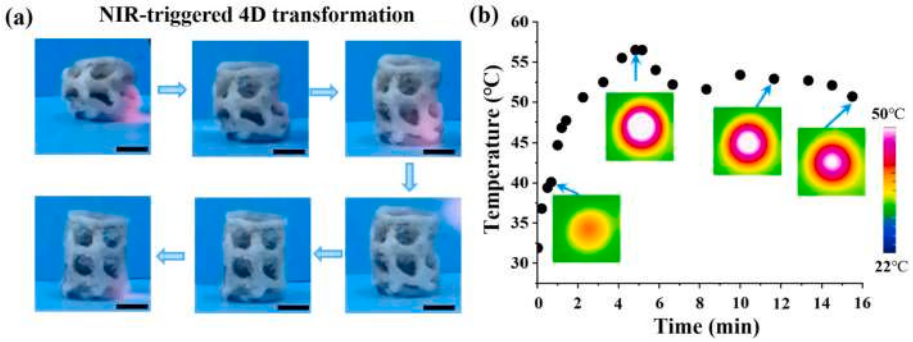

Fig. 8. (a) Dynamic, remote, and precisely controlled 4D transformation of GO functionalized PBS/PLA porous scaffold actuated by NIR laser at a power density of 5 W/cm^2. Scale bar: 5 mm. (b) Temperature evolution of GO functionalized PBS/PLA porous scaffold during 4D transformation.

Declaration of Competing Interest

The authors declare that they have no known competing financial interests or personal relationships that could have appeared to influence the work reported in this paper.

Acknowledgment

The authors gratefully acknowledge the financial supports provided by the National Natural Science Foundation of China (Grant Nos. 11632005 and 11672086). This work was also supported by the Fundamental Research Funds for the Central Universities.

Appendix A. Supplementary data

Supplementary data to this article can be found online at https://doi.org/10.1016/j.compstruct.2021.114729.

References

[1] Cera L, Gonzalez GM, Liu Q, Choi S, Chantre CO, Lee J, et al. A bioinspired and hierarchically structured shape-memory material. Nat Mater 2021;20(2):242–9.
[2] Wang W, Liu Y, Leng J. Recent developments in shape memory polymer nanocomposites: actuation methods and mechanisms. Coord Chem Rev 2016;320-321:38–52.
[3] Xin X, Liu L, Liu Y, Leng J. 4D printing auxetic metamaterials with tunable, programmable, and reconfigurable mechanical properties. Adv Funct Mater 2020; 30(43):2004226. https://doi.org/10.1002/adfm.v30.4310.1002/adfm.202004226.
[4] Falahati M, Ahmadvand P, Safaee S, Chang Y-C, Lyu Z, Chen R, et al. Smart polymers and nanocomposites for 3D and 4D printing. Mater Today 2020;40: 215–45.
[5] Xin X, Liu L, Liu Y, Leng J. Mechanical models, structures, and applications of shape-memory polymers and their composites. Acta Mech Solida Sin 2019;32(5): 535–65.
[6] Zhao Q, Li C, Shum HC, Du X. Shape-adaptable biodevices for wearable and implantable applications. Lab Chip 2020;20(23):4321–41.
[7] Wang J, Zhao Q, Wang Y, Zeng Qi, Wu T, Du X. Self-unfolding flexible microelectrode arrays based on shape memory polymers. Adv Mater Technol 2019; 4(11):1900566. https://doi.org/10.1002/admt.v4.1110.1002/admt.201900566.
[8] Zhao Q, Wang J, Cui H, Chen H, Wang Y, Du X. Programmed shape-morphing scaffolds enabling facile 3D endothelialization. Adv Funct Mater 2018;28(29): 1801027. https://doi.org/10.1002/adfm.v28.2910.1002/adfm.201801027.
[9] Lin C, Lv J, Li Y, Zhang F, Li J, Liu Y, et al. 4D-printed biodegradable and remotely controllable shape memory occlusion devices. Adv Funct Mater 2019;29(51): 1906569. https://doi.org/10.1002/adfm.v29.5110.1002/adfm.201906569.
[10] Nadgorny M, Ameli A. Functional polymers and nanocomposites for 3D printing of smart structures and devices. ACS Appl Mater Interfaces 2018;10(21):17489–507.
[11] Xin X, Liu L, Liu Y, Leng J. Origami-inspired self-deployment 4D printed honeycomb sandwich structure with large shape transformation. Smart Mater Struct 2020;29(6):65015. https://doi.org/10.1088/1361-665X/ab85a4.
[12] Zhang F, Xia Y, Liu Y, Leng J. Nano/microstructures of shape memory polymers: from materials to applications. Nanoscale Horiz 2020;5(8):1155–73.
[13] Tamay DG, Dursun Usal T, Alagoz AS, Yucel D, Hasirci N, Hasirci V. 3D and 4D printing of polymers for tissue engineering applications. Front Bioeng Biotechnol 2019;7. https://doi.org/10.3389/fbioe.2019.00164.
[14] Rastogi P, Kandasubramanian B. Breakthrough in the printing tactics for stimuli-responsive materials: 4D printing. Chem Eng J 2019;366:264–304.
[15] Kirillova A, Ionov L. Shape-changing polymers for biomedical applications. J Mater Chem B 2019;7(10):1597–624.
[16] González-Henríquez CM, Sarabia-Vallejos MA, Rodriguez-Hernandez J. Polymers for additive manufacturing and 4D-printing: materials, methodologies, and biomedical applications. Prog Polym Sci 2019;94:57–116.
[17] Shafranek RT, Millik SC, Smith PT, Lee C-U, Boydston AJ, Nelson A. Stimuli-responsive materials in additive manufacturing. Prog Polym Sci 2019;93:36–67.
[18] Miao S, Castro N, Nowicki M, Xia L, Cui H, Zhou X, et al.4D printing of polymeric materials for tissue and organ regeneration. Mater Today (Kidlington).2017;20: 577-91.
[19] Lin C, Zhang L, Liu Y, Liu L, Leng J. 4D printing of personalized shape memory polymer vascular stents with negative Poisson's ratio structure: a preliminary study. Sci China Technol Sci 2020;63(4):578–88.

[20] Zhao W, Zhang F, Leng J, Liu Y. Personalized 4D printing of bioinspired tracheal scaffold concept based on magnetic stimulated shape memory composites. Compos Sci Technol 2019;184:107866. https://doi.org/10.1016/j.compscitech.2019.107866.
[21] Lin C, Liu L, Liu Y, Leng J. 4D printing of bioinspired absorbable left atrial appendage occluders: a proof-of-concept study. ACS Appl Mater Interfaces 2021;13(11):12668–78.
[22] Zarek M, Mansour N, Shapira S, Cohn D. 4D printing of shape memory-based personalized endoluminal medical devices. Macromol Rapid Commun 2017;38(2):1600628. https://doi.org/10.1002/marc.v38.210.1002/marc.201600628.
[23] Liu H, Zhang J. Research progress in toughening modification of poly(lactic acid). J Polym Sci, Part B: Polym Phys 2011;49(15):1051–83.
[24] Lasprilla AJR, Martinez GAR, Lunelli BH, Jardini AL, Filho RM. Poly-lactic acid synthesis for application in biomedical devices — a review. Biotechnol Adv 2012;30(1):321–8.
[25] Saini P, Arora M, Kumar MNVR. Poly(lactic acid) blends in biomedical applications. Adv Drug Deliv Rev 2016;107:47–59.
[26] Shah Mohammadi M, Bureau MN, Nazhat SN. Polylactic acid (PLA) biomedical foams for tissue engineering. In: Netti PA, editor. Biomedical Foams for Tissue Engineering Applications: Woodhead Publishing;2014. p. 313-34.
[27] Tyler B, Gullotti D, Mangraviti A, Utsuki T, Brem H. Polylactic acid (PLA) controlled delivery carriers for biomedical applications. Adv Drug Deliv Rev 2016;107:163–75.
[28] Shi D, Kang Y, Zhang G, Gao C, Lu W, Zou H, et al. Biodegradable atrial septal defect occluders: a current review. Acta Biomater 2019;96:68–80.
[29] Huang Y, Kong JF, Venkatraman SS. Biomaterials and design in occlusion devices for cardiac defects: a review. Acta Biomater 2014;10(3):1088–101.
[30] Jompang L, Thumsorn S, On JW, Surin P, Apawet C, Chaichalermwong T, et al. Poly(lactic acid) and poly(butylene succinate) blend fibers prepared by melt spinning technique. Energy Procedia 2013;34:493–9.
[31] Deng Y, Thomas NL. Blending poly(butylene succinate) with poly(lactic acid): Ductility and phase inversion effects. Eur Polym J 2015;71:534–46.
[32] Lin C, Liu L, Liu Y, Leng J. The compatibility of polylactic acid and polybutylene succinate blends by molecular and mesoscopic dynamics. Int J Smart Nano Mater 2020;11(1):24–37.
[33] Gigli M, Fabbri M, Lotti N, Gamberini R, Rimini B, Munari A. Poly(butylene succinate)-based polyesters for biomedical applications: a review. Eur Polym J 2016;75:431–60.
[34] Wang L, Gramlich WM, Gardner DJ. Improving the impact strength of poly(lactic acid) (PLA) in fused layer modeling (FLM). Polymer 2017;114:242–8.
[35] Haq RHA, Rahman MNA, Ariffin AMT, Hassan MF, Yunos MZ, Adzila S. Characterization and Mechanical Analysis of PCL/PLA composites for FDM feedstock filament. IOP conference series. Materials Science and Engineering.2017;226:12038.
[36] Sezer HK, Eren O. 3D printing of MWCNT re-inforced ABS nano-composite parts with enhanced mechanical and electrical properties. J Manuf Processes 2019;37:339–47.
[37] Sodeifian G, Ghaseminejad S, Yousefi AA. Preparation of polypropylene/short glass fiber composite as Fused Deposition Modeling (FDM) filament. Results Phys 2019;12:205–22.
[38] Ma H, Jiang C, Zhai D, Luo Y, Chen Y, Lv F, et al. A bifunctional biomaterial with photothermal effect for tumor therapy and bone regeneration. Adv Funct Mater 2016;26(8):1197–208.
[39] Liu J, Cui L, Losic D. Graphene and graphene oxide as new nanocarriers for drug delivery applications. Acta Biomater 2013;9(12):9243–57.
[40] Chen G-Y, Pang D-W-P, Hwang S-M, Tuan H-Y, Hu Y-C. A graphene-based platform for induced pluripotent stem cells culture and differentiation. Biomaterials 2012;33(2):418–27.
[41] Lee J, Kim J, Kim S, Min D-H. Biosensors based on graphene oxide and its biomedical application. Adv Drug Deliv Rev 2016;105:275–87.
[42] Singh DP, Herrera CE, Singh B, Singh S, Singh RK, Kumar R. Graphene oxide: an efficient material and recent approach for biotechnological and biomedical applications. Mater Sci Eng C Mater Biol Appl 2018;86:173–97.
[43] Ostrowska J, Sadurski W, Paluch M, Tyński P, Bogusz J. The effect of poly(butylene succinate) content on the structure and thermal and mechanical properties of its blends with polylactide. Polym Int 2019;68(7):1271–9.
[44] Hu J, Albadawi H, Chong BW, Deipolyi AR, Sheth RA, Khademhosseini A, et al. Advances in Biomaterials and Technologies for Vascular Embolization. Adv Mater 2019;31(33):1901071. https://doi.org/10.1002/adma.v31.3310.1002/adma.201901071.
[45] Wong YS, Salvekar AV, Zhuang KD, Liu H, Birch WR, Tay KH, et al. Bioabsorbable radiopaque water-responsive shape memory embolization plug for temporary vascular occlusion. Biomaterials 2016;102:98–106.
[46] Liu Bo, Xu Z, Gao H, Fan C, Ma G, Zhang D, et al. Stiffness Self-Tuned Shape Memory Hydrogels for Embolization of Aneurysms. Adv Funct Mater 2020;30(22):1910197. https://doi.org/10.1002/adfm.v30.2210.1002/adfm.201910197.